Nuclear Inst. and Methods in Physics Research, A 1031 (2022) 166587

Contents lists available at ScienceDirect

Nuclear Inst. and Methods in Physics Research, A

journal homepage: www.elsevier.com/locate/nima

A beta–gamma radioxenon detection system using PIPS and CZT-Array

Yuanqing Fan [a,b,*], Xianyun Ai [a], Shilian Wang [b], Qi Li [b], Ying Wang [a], Yinzhong Chang [b], Yungang Zhao [b], Xinjun Zhang [b], Huaimao Jia [b]

[a] State Key Laboratory of NBC Protection for Civilian, Beijing, China
[b] CTBT Beijing National Data Centre and Beijing Radionuclide Laboratory, Beijing, China

ARTICLE INFO

Keywords:
Radioxenon
CTBT
PIPS
CZT
Beta–gamma coincidence
MDA

ABSTRACT

Radioxenon monitoring is one of the important methods used by the Comprehensive Nuclear-Test-Ban Treaty Organization (CTBTO) to detect a clandestine nuclear weapon test. Many radioxenon detection systems have been developed in the past few decades. The disadvantages such as bad energy resolution, memory effect, and large size influence the performance of these systems. This work introduces a new detection system that utilizes a PIPSCell and two CZT-Arrays for radioxenon monitoring. Signals from ten detectors are processed and coincidence events are identified via the electronics based on time-stamped list mode. This compact system has good radiation detection resolution at room temperature and high detection sensitivity for both electron and gamma-ray. Preliminary ^{137}Cs and ^{131m}Xe are used to calibrate the energy and efficiency of the system. Combined with the simulation results the minimum detection activity of four radioxenon were assessed.

1. Introduction

In order to prevent the proliferation of nuclear weapons, promote nuclear disarmament and enhance the international peace and security, the Comprehensive Nuclear-Test-Ban Treaty (CTBT) was opened to signature in 1996 [1]. From then on, the International Monitoring System (IMS) that involves four monitoring technologies, radionuclide, seismic, hydroacoustic, and infrasonic has been deployed to verify the compliance with the treaty [2].

Within the IMS of the CTBT a radionuclide monitoring network consisting of 80 globally distributed radionuclide stations and 16 radionuclide laboratories has been implemented. All stations shall be capable of monitoring the presence of relevant radionuclide particulate matter in the atmosphere. Forty of these stations shall also be capable of monitoring the presence of relevant radioxenon isotopes, simultaneously, following the entry into the force of the CTBT [3].

Due to the large production cross sections in fission, the suitable half-lives, the chemical inertness and the gaseous state, ^{131m}Xe (11.84d), ^{133m}Xe (2.19d), ^{133}Xe (5.24d), and ^{135}Xe (9.14 h) [4] are in the list of the CTBT relevant nuclides, namely the relevant radioxenon isotopes.

Radioxenon monitoring has been the focus in the radionuclide monitoring since the year 2000, and several advanced xenon monitoring systems have been developed and equipped in the radionuclide stations to monitor the radioxenon automatically. The systems are ARSA, SAUNA, ARIX, and the SPALAX [5–8]. Generally these systems have two main functions, including xenon sampling and radioxenon measurement. In the xenon sampling process these systems collect, concentrate, and purify the xenon sample in atmosphere. As to the radioxenon measurement, two measuring techniques, HPGe gamma spectrometry and coincidence detection spectrometry, have been developed.

The activity measurements of ARSA, SAUNA, and ARIX are based on the beta–gamma coincidence mode where the electrons and gamma-ray are detected by a cylindrical plastic scintillator cell and a surrounding NaI(Tl) crystal, respectively. Initially the activity measurement apparatus of SPALAX is based on HPGe gamma spectrometry, and then it has been upgraded to the beta–gamma coincidence mode with the new generation SPALAX (SPALAX™ NG) [9].

The four systems have been used to measure the radioxenon samples successfully for many years in the IMS. However these systems possess some imperfections, including bad energy resolution, memory effect (ARSA, SAUNA and ARIX), bulkiness (SPALAX), etc. Then some modifications were applied to remove these imperfections, for example, the NaI(Tl) detectors was replaced by HPGe detectors due to the excellent energy resolution or by CZT due to the good energy resolution when operated at room temperature [10–14], the plastic scintillator was replaced by PIPS detector due to the better energy resolution and weaker memory effect [15], the memory effect of plastic scintillator detectors was reduced by surface coating or using stilbene gas cell [14,16]. Additionally some measuring techniques based on HPGe gamma spectrometry, for example, the anti-cosmic ray gamma spectrometry and the Compton-suppression spectrometry are used to improve the detection sensitivity by reducing the background [17,18].

* Corresponding author at: State Key Laboratory of NBC Protection for Civilian, Beijing, China.
E-mail addresses: yuanqing.fan@nrl.org.cn (Y. Fan), aixy@ihep.ac.cn (X. Ai), shilian.wang@nrl.org.cn (S. Wang).

https://doi.org/10.1016/j.nima.2022.166587
Received 6 November 2021; Received in revised form 28 February 2022; Accepted 6 March 2022
Available online 16 March 2022

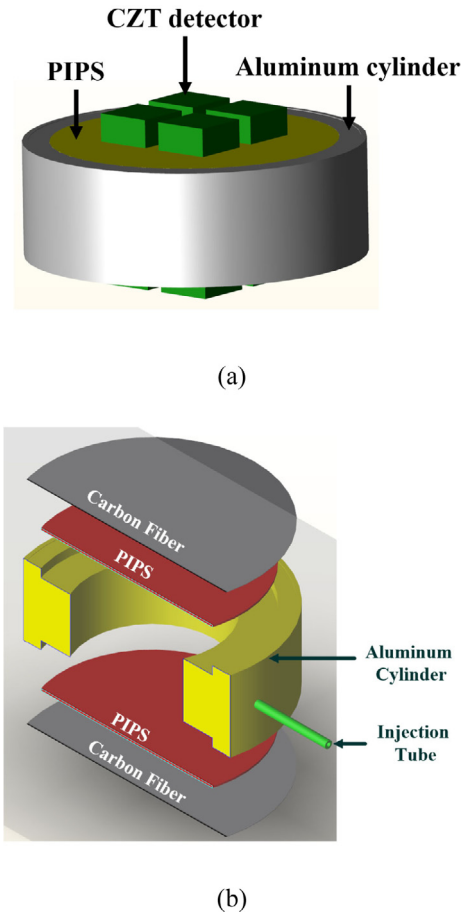

Fig. 1. (a) Schematic of the detection system using PIPS and CZT-Array; (b) Schematic of the PIPSCell.

As to these modified systems, the radioxenon detection system using PIPSBox and CZT developed by school of Nuclear Science and Engineering of Oregon state university are excellent because of the good resolution, the simple readout electronics, the compact configuration and the weak memory effect. However, since only two planar CZT detectors were utilized to detect the gamma radiation emitted by the radioxenon, the sensitivity of the system is limited by the low detection efficiency of gamma. In this paper a beta–gamma radioxenon detection system using PIPS and CZT-Array composed of eight CZT detectors is introduced. With this detection system coincidence measurements of ^{131m}Xe was performed. The MDCs of four radioxenon were also estimated preliminary.

2. Simulation

The detection system is comprised of a PIPSCell and two CZT-Arrays (Fig. 1). The PIPSCell is utilized to detect electron and contain the radioxenon gas. In the PIPSCell two Passivated implanted planar silicon (PIPS) wafers are fixed on the top and bottom of an aluminum cylinder, and two pieces of carbon fiber outside of the PIPS wafers is used to seal the cell inside the aluminum cylinder. The CZT-Arrays are used as the gamma-ray detectors. Two CZT ($1 \times 1 \times 0.5$ cm^3) Arrays locates on the top and the bottom of PIPSCell respectively.

SPALAX™ NG can extract more than 6 mL of pure xenon during 12 h, while SAUNA III can collect 4 samples during 24 h and xenon volume of each sample is about 3 mL. In order to contain the xenon sample on negative pressure and reduce the leakage of xenon sample into the atmosphere during the measurement, the PIPSCell is designed with the active volume of 15 mL.

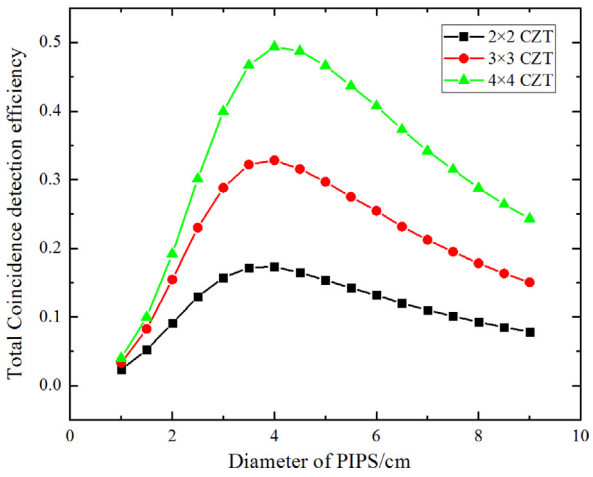

Fig. 2. Total coincidence detection efficiency.

The key decay properties of xenon isotopes of interest was listed in Table 1. ^{131m}Xe and ^{133m}Xe emit internal-conversion electrons (CE) coincident with X-rays, while ^{133}Xe and ^{135}Xe emit beta-rays coincident with gamma-rays and X-rays. The electron detection efficiency ε_β is defined as the ratio of the electron (internal-conversion electron or beta-ray) number that interact with PIPS to the electron number emitted by radioxenon isotope. Similarly the photon detection efficiency ε_γ is defined as the ratio of the photon (X-ray and gamma-ray) number that interact with CZT detectors to the photon number emitted by radioxenon isotope. The coincidence detection efficiency $\varepsilon_{\beta\gamma}$ is the product of ε_β and ε_γ.

In order to obtain the optimized design scheme, SuperMC program was used to simulate the detection efficiency of beta-ray (average energy) and gamma-ray emitted by ^{133}Xe [19]. To certain active volume (15 mL), the ε_β, ε_γ, and $\varepsilon_{\beta\gamma}$ of the integral detection system for radioactive xenon sample is related with the dimension of PIPS. A series of PIPSCell models that have different diameters and corresponding the thicknesses of the active volume are built. In the models the thickness of PIPS wafer is 500 um and its dead layer is 1 um. In the models ^{133}Xe atoms fill the whole cylinder active volume of the PIPSCell. The original source particles include 81 keV characteristic gamma-ray and 100 keV (the average energy of beta ray) electron and all the particles are emitted from isotropic source of ^{133}Xe atoms. The energy threshold of the PIPS and CZT detectors is set as 5 keV in the tally.

The total coincidence detection efficiency is shown in Fig. 2. No matter how many detectors are arranged in a CZT arrays, the maximum of coincidence detection efficiency appears when the radius of PIPS is about 4 cm. 1. The diameter of PIPS is 3.5 cm to establish the PIPSCell to avoid the bad energy resolution induced by excessive leakage current with larger area. Then the inner radius, the external diameter and the height of the aluminum cylinder is 3.5, 5.0 and 1.56 cm respectively.

Obviously the more CZT detectors are arranged, the higher is the coincidence detection efficiency of the detection system. Considering the energy resolution and economic factor, it is unpractical to use lots of CZT. To the $2 \times 2, 3 \times 3$ and 4×4 CZT arrays, the mean coincidence detection efficiency that is the coincidence detection efficiency divided by the quantity of CZT are shown in Fig. 3. Due to the highest mean coincidence detection efficiency, the two 2×2 CZT arrays is adopted.

Fig. 4 shows the simulated ε_β, ε_γ, and $\varepsilon_{\beta\gamma}$ of the detection system using two 2×2 CZT arrays when the diameter of PIPS varies from 1 to 9 cm. When the diameter of PIPS becomes larger, the efficiency of PIPS increases continuously, and the efficiency of CZT arrays increases first and then decreases. The coincidence detection efficiency also increases first and then decreases, hence a maximum appears when the diameter of PIPS is about 4 cm.

Table 1
Decay properties of xenon isotopes of interest [20].

Isotope	Half-life	X-ray /keV	Branching ratio/%	Gamma /keV	Branching ratio/%	CE/keV	Branching ratio/%	Beta/keV average/end point
^{131m}Xe	11.962 d	30.38	54.47	163.930	1.942	129.366	61.4	
^{133m}Xe	2.198 d	30.46	56.34	233.219	10.16	198.655	63.5	
^{133}Xe	5.2474 d	30.9	47.63	80.9979	37.0	45.0133	52.9	100.6/346.4
^{135}Xe	9.14 h	32.18	5.94	249.794	90	213.91	5.6	249.793/910

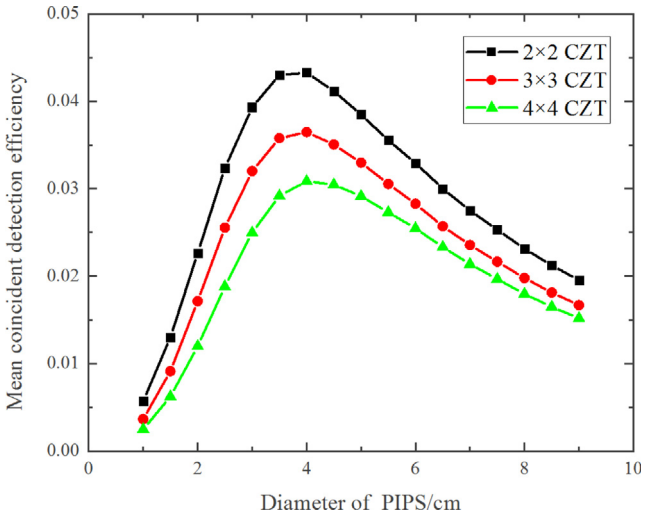

Fig. 3. Mean coincidence detection efficiency.

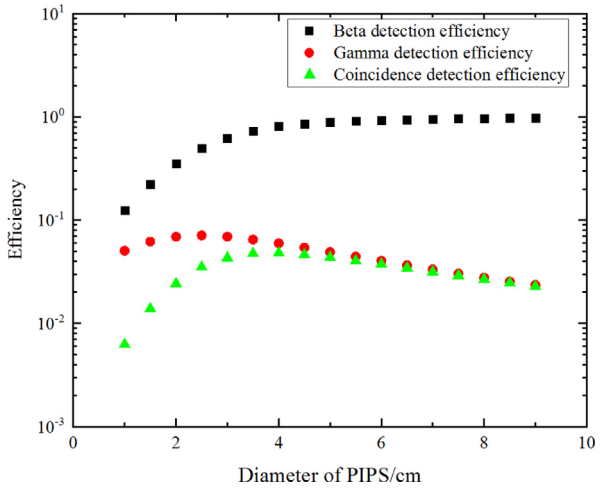

Fig. 4. Simulated ε_{β}, ε_{γ} and $\varepsilon_{\beta\gamma}$ of the detection system using two 2 × 2 CZT.

3. PIPSCell

The PIPSCell is manufactured by Chengdu Jingwei Science and Technology Co., Ltd [21]. The PIPSCell consists in two PIPS wafers and an aluminum cylinder. The aluminum cylinder was 3.5 cm in inner diameter, 5 cm in external diameter and 2.0 cm high. Two wafers are arranged face-to-face and coaxial with the aluminum cylinder. The distance between two wafers is 1.6 cm. The active area and the thickness of the wafers is about 960 mm^2 and 500 μm respectively. The thickness of the wafer is enough to absorb the electrons emitted by the radioxenon of interest. On the top and bottom of aluminum cylinder the PIPSCell is sealed with 600 μm carbon fiber. The PIPSCell are mounted on a PCB-based preamplifier that provide 50 V bias voltages for PIPS and amplify the signals. The PIPSCell and the PCB-based preamplifier are shown in Fig. 5.

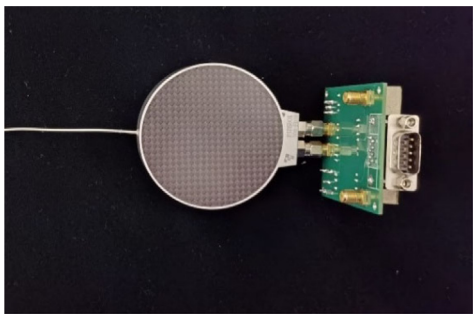

Fig. 5. The assembled PIPSCell mounted on the PCB.

4. CZT-Array

Normally the energy resolution of CZT detectors is less than 2% at 661.7 keV and better than the scintillator detectors that have been utilized by other beta–gamma coincidence system. Unlike HPGe detectors, CZT detectors can be used at room temperature, so the troublesome maintenance of liquid nitrogen supply or bulky cooling system can be avoided. Due to aforementioned advantages CZT detectors are chosen to detect the photon. In order to improve the detection efficiency for photon, two CZT-Arrays composed of eight hemispherical CZT detectors are utilized. The CZT-Arrays are provided by Northwestern Polytechnical University. The dimension of every CZT crystal is 1 × 1 × 0.5 cm^3, and four CZT crystal are packaged into one 2 × 2 CZT array. The CZT array is cased in aluminum shell with 0.5 mm beryllium window. The two CZT-Arrays and the inner structure of the CZT-Array are shown in Fig. 6.

5. Electronics

The electronics based on time-stamped list mode is provided by Chengdu University of Technology. The schematic drawing of electronics is shown in Figs. 7A and 7B. The analog signals from the preamplifiers of ten detectors (two PIPS and eight CZT) are convert to digital signals respectively. Then information of each signal, such as detector ID, arrival time, pulse amplitude, pulse rise time, etc. is extracted as an independent data packet. All the event data packets are sent to the FPGA-based digital processing module. The amplification and shaping of signal is processed in the FPGA digital processing module. In order to ensure the time synchronization, a 200 MHz synchronous clock is employed to time-stamp each event data packet. The optimal coincidence timing window is 2.0 μs. The spectra of PIPS and CZT detectors can be plotted automatically by the host computer software.

6. Experiment

6.1. Calibration

Two CZT-Arrays was calibrated using ^{137}Cs and ^{152}Eu point source. In order to get good energy resolution (*FWHM*) in the summing spectrum, the full energy peaks (FEP) of 662 keV of eight CZT crystals were located at identical channel by adjusting the parameters in the host computer software (Fig. 8). The energy resolution of 2.5% was observed for the 662 keV FEP in the summing spectrum of CZT-Arrays.

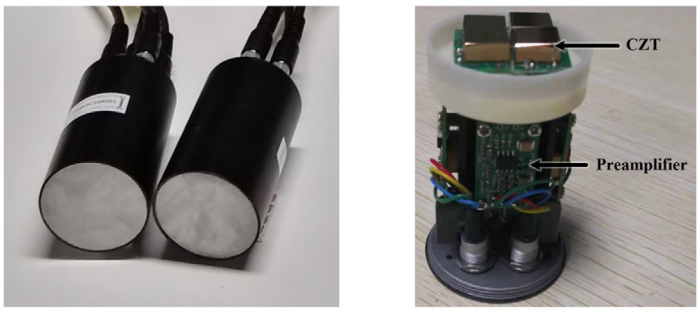

Fig. 6. (A) Two CZT-Arrays. (B) Inner structure of CZT-Array.

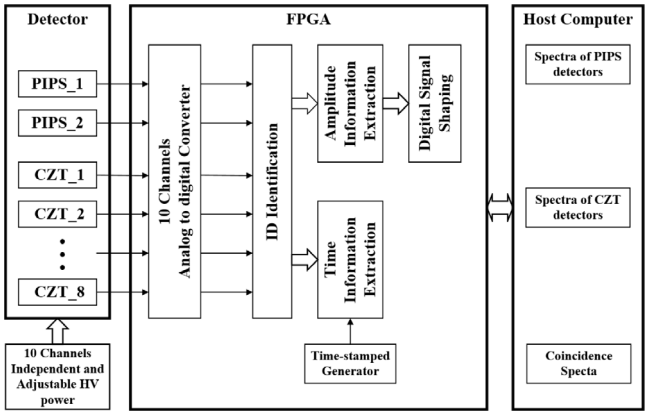

Fig. 7A. Diagram of electronics based on FPGA. The analog signals from the preamplifiers of eight CZT and two PIPS are convert into digital signals in ADC model and given an ID numbers by ID Identification model. Then the amplitude of digital signals are extracted and amplified. The amplified signals with identical ID number are acquired and spectrum is construct by control software in the host computer.

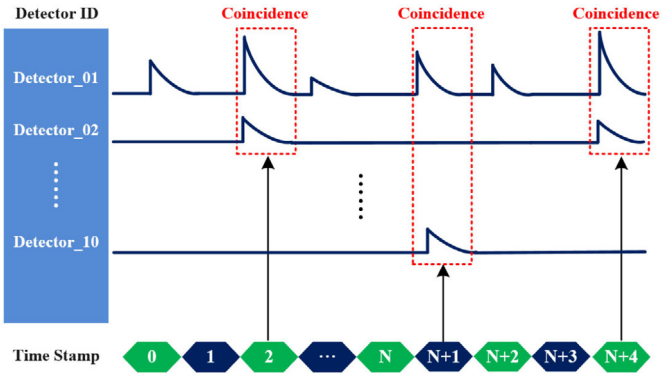

Fig. 7B. Schematic diagram of the coincidence firmware in FPGA. The digital signals are time-stamped by the Time-stamped generator in FPGA. The interval of the time-stamp is 5 ns. When signals from two or more detectors fall into the identical interval, these signals are coincident. The amplitude information of these coincident signals are used to construct 2-D spectrum.

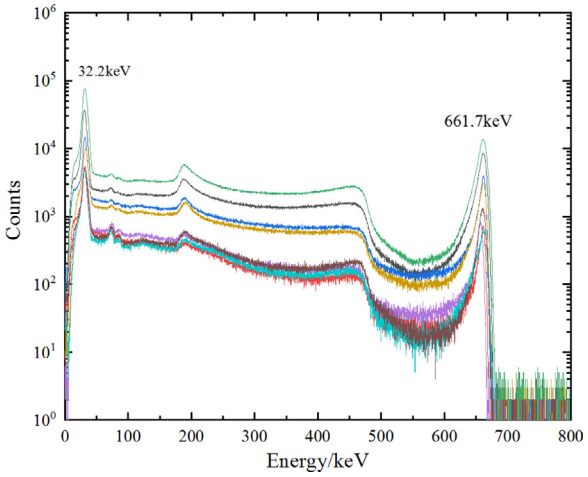

Fig. 8. The 662 keV FEP located at identical channel of eight CZT detectors.

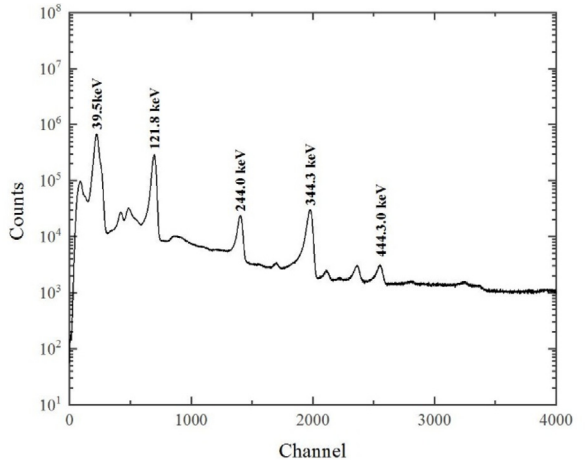

Fig. 9. The summing spectrum of ^{152}Eu acquired by eight CZT detectors. The count in every channel of the summing spectrum is the summation of count in identical channel of eight spectra acquired by CZT detectors.

Then ^{152}Eu was used to calibrate the energy at 39.5, 121.8, 244.0, 344.3, 444.3 keV. The summing spectrum of ^{152}Eu acquired by eight CZT detectors is shown in Fig. 9 and the resolution calibration using ^{152}Eu and ^{137}Cs is shown in Fig. 10.

The PIPSCell was calibrated with the Compton scattering calibration technique [22,23]. As an intense ^{137}Cs source is located beside the PIPSCell, the incident gamma-ray of 661.7 keV scatters in the PIPS producing a recoil electron that deposits in the PIPS, simultaneously the scattering photon can be detected in the CZT-Arrays. Then a two-dimensional (2D) beta–gamma coincidence spectrum is obtained by displaying the CZT arrays pulse height versus the summed pulse heights of the two PIPS. The two-dimensional beta–gamma energy spectrum of ^{137}Cs is shown in Fig. 11. Apparently the dense dots distributed along the diagonal line are generated due to the coincidence detection to the Compton scattering of the 661.7 keV gamma ray from ^{137}Cs. In the 2D beta–gamma coincidence spectrum the gamma energy axis had been

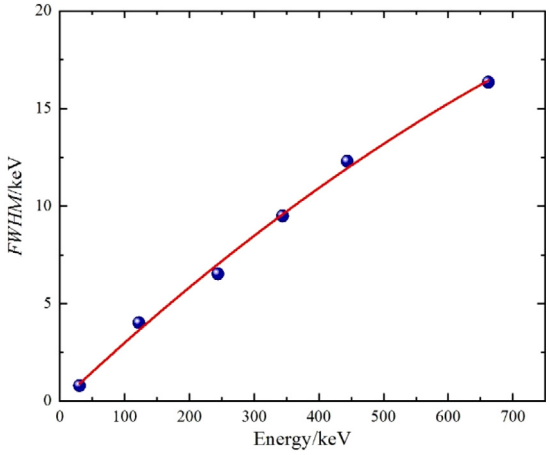

Fig. 10. Resolution calibration curve.

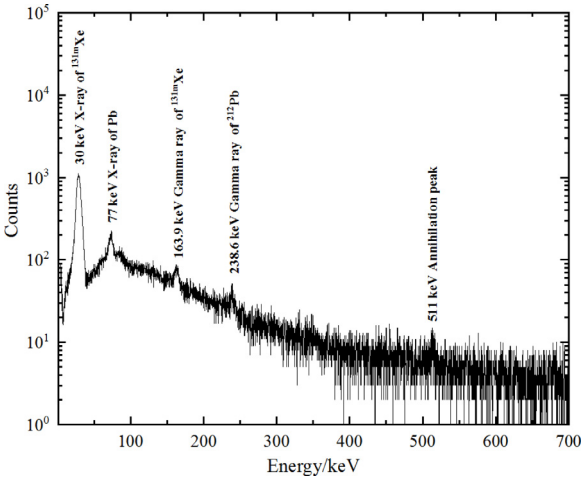

Fig. 12. The ^{131m}Xe summing spectrum acquired by CZT-Arrays.

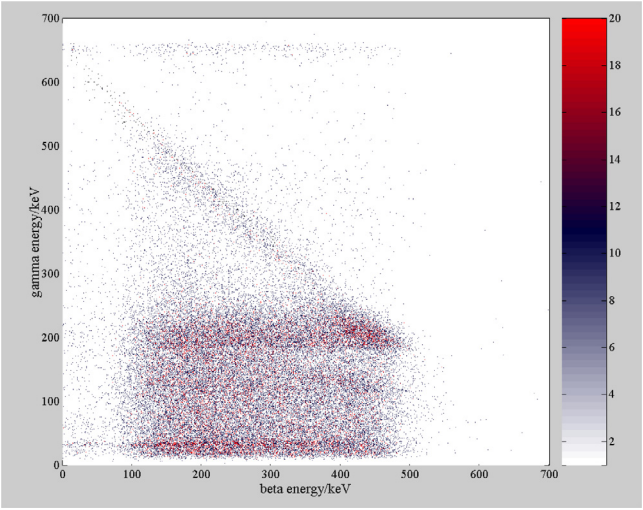

Fig. 11. The 2-D beta–gamma energy spectrum of ^{137}Cs.

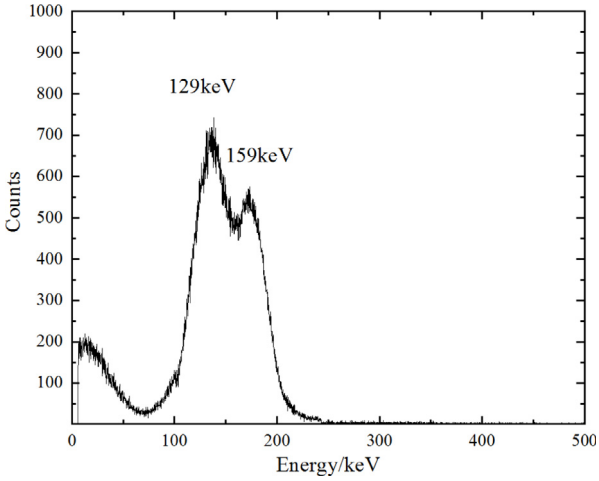

Fig. 13. The spectrum of ^{131m}Xe acquired by PIPSCell.

calibrated with ^{137}Cs and ^{152}Eu source. The beta energy axis can be calibrated with the recoil electron energy that is given by the energy of the incident gamma-ray minus the energy of the scattered gamma-ray. Finally, one can see three regions formed by dense dots beneath the diagonal line. The dots in the horizontal region at 200 keV gamma energy are generated due to the backscatter of 661.7 keV photons in the CZT arrays and the successive Compton scattering in the PIPS. The dots in the horizontal region at 30 keV gamma energy are generated due to the accidental coincidence between the 30 keV X-rays detected by CZT Arrays and recoil electrons of 661.7 keV photons detected by PIPS. The dots in the region that locates between the aforementioned two regions are generated due to the successive Compton scatterings in PIPS and CZT arrays.

6.2. ^{131m}Xe Sample preparation

In order to assess the performance of the prototype, a reference radioxenon sample was prepared. Generally the four relevant radioxenon isotopes are produced by irradiate ^{235}U or pure xenon targets in neutron field. In this work ^{131m}Xe can be obtained by collecting the daughter of ^{131}I.

^{131}I is a common medical radionuclide and has two daughters, radionuclide ^{131m}Xe and stable nuclide ^{131}Xe, so the ^{131}I+ (NaI) solution is used to prepare ^{131m}Xe sample [24]. At first some ^{131m}Xe gas mixed with ^{131}I and moisture was drawn off with a syringe from the gaseous phase of the vessel containing $^{131}I^{+}$ (NaI) solution. In order to remove the $^{131}I^{+}$, the gas was inject into a filter filled with sponge that had been soaked in $AgNO_3$ solution. Then the gas flew through another filter filled with silica gel desiccant to remove the moisture and was absorbed into a vacuum vessels. At last the pure and dry ^{131m}Xe sample added in carrier gas was separated into PIPSCell and a set of inner gas proportional counters in parallel. The activity concentration of the ^{131m}Xe sample was determined with the internal gas proportional counters.

6.3. ^{131m}Xe Measurement

The ^{131m}Xe in the PIPSCell was measured with the system. The spectra of the PIPS, CZT-Arrays and 2D beta–gamma coincidence spectrum were acquired simultaneously. Fig. 12 shows ^{131m}Xe summing spectrum acquired by CZT-Arrays. Compared with the FEP at 30 keV X-ray, the FEP at 163.9 keV is not prominent due to the small emission probability of 163.9 keV gamma ray. In the summing spectrum the energy resolution is 17% at 30 keV, better than 32% of NaI(Tl) detector but worse than 2% of HPGe detector [9,24].

The beta spectrum of ^{131m}Xe acquired by PIPSCell is shown in Fig. 13. In the spectrum a doublet peak of conversion electrons appears near 129 ke. After the analysis of multiple peaks, two peaks can be identified at 129 keV and 159 keV respectively. The energy resolution

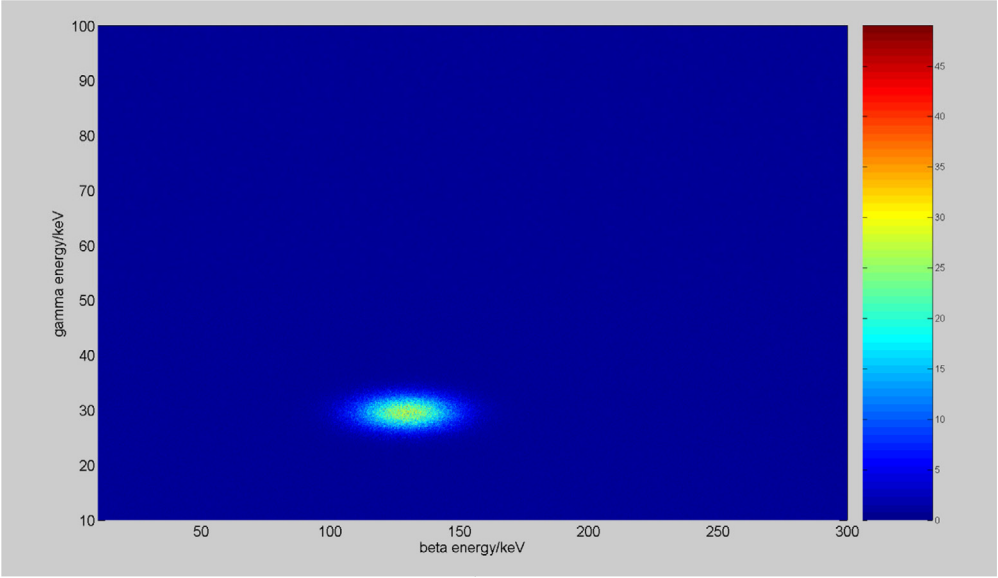

Fig. 14. The 2D beta–gamma coincidence spectrum of ^{131m}Xe.

of PIPSCell was 19% at 129 keV. The peak in the low energy zone is due to the electronic noise in the PIPSCell.

A 2D beta–gamma coincidence spectrum of ^{131m}Xe acquired with the system is shown in Fig. 14. In the spectrum the beta–gamma coincidence events from ^{131m}Xe are recorded in an elliptical region. Due to the good energy resolution, the peaks produced by the gamma-rays and the electrons can be considered approximately to follow Gaussian distribution. The pulse heights of the coincidence events follow 2D Gaussian distribution. Then an elliptical region appears when the pulse heights of the coincidence events are projected to the zero contour plane. Two peaks can be identified at 129 keV and 159 keV in the beta spectrum of ^{131m}Xe, but only 129 keV electron is coincident with the 30 keV X-ray. Therefore there is just one coincidence region.

The activity concentration of ^{131m}Xe reference sample has been determined with the inner gas proportional counters, whereas the volume of ^{131m}Xe in the cell has been determined by the volume ratio of the PIPSCell to the proportional counters. Therefore coincidence efficiency $\varepsilon_{\beta\gamma}$ is determined to be 6.32 ± 5.00% for ^{131m}Xe via experiment. The simulated coincidence efficiency is 6.80% and 7.58 percent larger than the experimental coincidence efficiency.

6.4. Minimum detectable activity

Radioxenon measurement systems should be sensitive enough to detect the trace amount of radioxenon. The minimum detectable activity (MDA) is an important performance index to assess the sensitivity of the measuring apparatus. MDA for beta–gamma coincidence system can be calculated as [25]

$$MDA = \frac{2.71 + 4.65\sqrt{\mu_B}}{T\varepsilon_\beta P_\beta \varepsilon_\gamma P_\gamma} \frac{\lambda_i t_C}{1 - e^{-\lambda_i t_C}} \quad (1)$$

where

$\sqrt{\mu_B}$ the standard deviation of the background with empty PIPSCell at the region of interest (ROI),

T the acquisition live time (s),

ε_β the electron detection efficiency,

ε_γ the gamma-ray detection efficiency,

P_β the branching ratio of electron,

P_γ the branching ratio gamma ray,

λ_i the decay constant for the isotope i (s^{-1}), and

t_C the clock time of acquisition (s).

A 7 day background measurement was performed using the system. The counts in the ROIs of certain radioxenon are calculated to assess the MDAs of 3 day measurement. A beta–gamma radioxenon detection system with a PIPSBox in sandwich between two high purity germanium detectors had been developed and assessed by French CTBTO laboratory [26]. The MDAs of four radioxenon for both systems are list in Table 2. It is obvious that the latter's MDAs is smaller than the former's. Firstly the radioxenon detection system of French CTBTO laboratory has bigger detection volume for electron and photon, therefore both ε_β and ε_γ is higher in Eq. (1). Undoubtedly the bigger volume of detector results in the more background count. However with beta–gamma coincidence mode only the volume growth of PIPS results in the increase of background count from the environmental radioactivity. Secondly the good energy resolution of electron and photon detectors is primary cause of high detection sensitivity of the latter. For example, the electron energy resolution is 19% and 9% at 129 keV for the former and the latter respectively, moreover the photon energy resolution is 17% and 2% at 30 keV for the former and the latter respectively. Good energy resolution in a radioxenon detection system means the narrow ROIs for the radioxenon in the background spectrum. The narrow ROIs reduce interference from other coincidence sources and allow for the detection of radioxenon at lower concentrations [15].

7. Conclusion

A beta–gamma radioxenon detection system composed a PIPSCell and two CZT-Arrays was introduced. The analog signals from the ten detectors were read out and converted to digital signals using a FPGA-based twelve-channel digital processing module. A ^{137}Cs source and ^{131m}Xe reference sample were used to calibrate the energy and efficiency of detection system. The coincidence efficiency $\varepsilon_{\beta\gamma}$ is 6.32 ± 0.50% for ^{131m}Xe via experiment. Additionally the MDAs were assessed for the four radioxenon. For a 3 day measurement, MDA for ^{131m}Xe, ^{133}Xe, ^{133m}Xe and ^{135}Xe is 1.5, 1.5, 1.8 and 4.4 mBq respectively.

In order to improve the electron energy resolution, the PIPS detector with better performance will be used to compose a new PIPSCell in the future. Additional works will be performed to calibrate the energy and the efficiency using ^{133}Xe, ^{133m}Xe and ^{135}Xe samples and assess the MDAs again. The anti-cosmic ray detectors will be used to reduce the background and improve the detection sensitivity of the system.

Table 2
MDAs for each radioxenon isotope of interest. The efficiency for ^{133}Xe, ^{133m}Xe and^{135}Xe was determined via SuperMC simulation and scaled to the ratio of the experimentally determined efficiency and the simulated efficiency of ^{131m}Xe for the system based on PIPSCell and CZT-Arrays.

	^{131m}Xe	^{133}Xe	^{133m}Xe	^{135}Xe
Beta–gamma radioxenon detection system based on PIPSCell and CZT-Arrays	1.5 mBq	1.5 mBq	1.8 mBq	4.4 mBq
Beta–gamma radioxenon detection system based on PIPSBox and two HPGe detectors	0.3 mBq [26]	0.3 mBq [26]	0.4 mBq [26]	0.6 mBq [26]

CRediT authorship contribution statement

Yuanqing Fan: Conceptualization, Methodology, Writing – original draft. **Xianyun Ai:** Methodology, Writing – review & editing. **Shilian Wang:** Conceptualization, Writing – review & editing. **Qi Li:** Investigation, Data curation. **Ying Wang:** Methodology, Supervision. **Yinzhong Chang:** Sample preparation. **Yungang Zhao:** Data curation, Validation. **Xinjun Zhang:** Visualization, Software. **Huaimao Jia:** Visualization, Validation.

Declaration of competing interest

The authors declare that they have no known competing financial interests or personal relationships that could have appeared to influence the work reported in this paper.

Acknowledgments

This work is partly supported by the National Natural Science Foundation of China through grant No. 12075318.

References

[1] CTBTO, Website of the preparatory commission for the comprehensive nuclear test-ban treaty organization, 2013, http://www.ctbto.org/.
[2] J.D. Sullivan, The comprehensive test ban treaty, Phys. Today 151 (1998) 23.
[3] Protocol to the comprehensive nuclear test-ban treaty, https://www.ctbto.org/the-treaty/treaty-text/.
[4] R.B. Firestone, Table of Isotopes CD-ROM, Eighth Edition, Lawrence Berkeley National Laboratory, University of California., 1998, Update.
[5] J. McIntyre, K. Abel, T. Bowyer, J. Hayes, T. Heimbigner, M. Panisko, P. Reeder, R. Thompson, Measurements of ambient radioxenon levels using the automated radioxenon sampler/analyzer (ARSA), J. Radioanal. Nucl. Chem. 248 (2001) 629–635.
[6] A. Ringbom, T. Larson, A. Axelsson, K. Elmgren, C. Johansson, Sauna-a system for automatic sampling, processing, and analysis of radioactive xenon, Nucl. Instrum. Methods Phys. Res. A 508 (2003) 542–553, http://dx.doi.org/10.1016/S0168-9002(03)01657-7.
[7] V.V. Prelovskii, N.M. Kazarinov, A. Yu. Donets, V. Yu. Popov, I. Yu. Popov, N.V. Skirda, The ARIX-03F mobile semiautomatic facility for measuring low concentrations of radioactive xenon isotopes in air and subsoil gas, Instrum. Exp.Tech. 50 (3) (2007) 393–397.
[8] J.P. Fontaine, F. Pointurier, X. Blanchard, T. Taffary, Atmospheric xenon radioactive isotope monitoring, J. Environ. Radioact. 72 (2004) 129–135.
[9] G. Le Petit, A. Cagniant, P. Gross, G. Douysset, S. Topin, J.P. Fontaine, T. Taffary, C. Moulin, Spalax ™ new generation: A sensitive and selective noble gas system for nuclear explosion monitoring, Appl. Radiat. Isot. 103 (2015) 102–114, http://dx.doi.org/10.1016/j.apradiso.2015.05.019.
[10] Q. Li, S.L. Wang, H.M. Jia, Y.G. Zhao, Y.Q. Fan, X.J. Zhang, A plastic scintillator gas detector designed for radioxenon isotopes measurement with a high electron detection efficiency, Nucl. Instrum. Methods Phys. Res. A 988 (2021) 164939.
[11] L. Ranjbar, A.T. Farsoni, E.M. Becker, A CZT-based radioxenon detection system in support of the comprehensive nuclear-test-ban treaty, J. Radioanal. Nucl. Chem. 310 (2016) 969–978, http://dx.doi.org/10.1007/s10967-016-4872-8.
[12] S.A. Czyz, A.T. Farsoni, A radioxenon detection system using CdZnTe, An array of SiPMs, and a plastic scintillator, J. Radioanal. Nucl. Chem. 313 (2017) 131–140, http://dx.doi.org/10.1007/s10967-017-5287-x.
[13] S.A. Czyz, A.T. Farsoni, L. Ranjbar, A prototype detection system for atmospheric monitoring of xenon radioisotopes, Nucl. Instrum. Methods Phys. Res. A (2017) http://dx.doi.org/10.1016/j.nima.2017.10.044.
[14] H.R. Gadey, A.T. Farsoni, S.A. Czyz, K.D. McGee, A stilbene - CdZnTe based radioxenon detection system, J. Environ. Radioact. 204 (2019) 117–124, http://dx.doi.org/10.1016/j.jenvrad.2019.03.027.
[15] S.A. Czyz, A.M. Alhawsawi, A.T. Farsoni, H.R. Gadey, L. Ranjbar, M.A. Mannino, K.D. McGee, A radioxenon detection system using PIPS and CZT, J. Radioanal. Nucl. Chem. (2018) http://dx.doi.org/10.1007/s10967-018-6367-2.
[16] L. Bläckberg, A. Fay, I.Jõgi, S. Biegalski, M. Boman, K. Elmgren, T. Fritioff, A. Johansson, L. Mårtensson, F. Nielsen, A. Ringbom, M. Rooth, H. Sjöstrand, M. Klintenberg, Investigations of surface coatings to reduce memory effect in plastic scintillator detectors used for radioxenon detection, Nucl. Instrum. Methods Phys. Res. A 656 (2011) 84–91.
[17] Q. Li, S.L. Wang, Y.Q. Fan, Y.G. Zhao, H.M. Jia, X.J. Zhang, J. Wang, W.X. Yu, Radioactivity measurement of xenon isotope by anti-cosmic ray γ spectrometer, At. Energy Sci. Technol. 51 (2017) 330–337.
[18] Y.Q. Fan, Q. Li, Y. Wang, Y.G. Zhao, X.J. Zhang, H.M. Jia, Y.Z. Chang, S.J. Liu, X.Y. Ai, S.L. Wang, Assessment of a compton-suppressed spectrometer for measurement of radioactive xenon isotopes, Appl. Radiat. Isot. 172 (2021) 109669.
[19] Frontier Development of Science, Supermc user's manual, 2020.
[20] K. Khrustalev, J. Wieslander, M. Auer, A. Gheddou, Calibration of low-level beta–gamma coincidence detector systems for xenon isotope detection, Appl. Radiat. Isot. 109 (2016) 418–424, http://dx.doi.org/10.1016/j.apradiso.2015.11.032.
[21] Chengdu Jingwei Science and Technology Co., LTD, http://www.techjw.com.
[22] P. Reeder, T. Bowyer, J. McIntyre, et al., Gain calibration of a beta/gamma coincidence spectrometer for automated radioxenon analysis, Nucl. Instrum. Meth. Phys. Res. Sect. A 521 (2004) 586–599, http://dx.doi.org/10.1016/j.nima.2003.11.195.
[23] Q. Li, Y.Q. Fan, S.J. Liu, Y.Z. Chang, Y.G. Zhao, S.L. Wang, Preparation for pure ^{131m}Xe sample, Nucl. Electron. Detect. Technol. 37 (2017) 696–699.
[24] P.L. Reeder, T.W. Bowyer, J.I. McIntyre, W.K. Pitts, A. Ringbom, C. Johansson, Gain calibration of a beta/gamma coincidence spectrometer for automated radioxenon analysis, Nucl. Instrum. Methods Phys. Res. A 521 (2004) 586–599, http://dx.doi.org/10.1016/j.nima.2003.11.195.
[25] CTBTO, Certification and surveillance assessment of radionuclide laboratories for particulate and noble gas sample analysis, 2012, CTBT/PTS/INF.96/Rev.9.
[26] O. Delaune, A. Cagniant, P. Gross, G. Douysset, J.P. Fontaine, G. Le Petit, Low-level laboratory measurement of xenon radionuclides: Electron-photon versus photon measurements, Appl. Radiat. Isot. 103 (2015) 102–114.